Modeling over-ageing in Al-Mg-Si alloys by a multi-phase CALPHAD-coupled Kampmann-Wagner Numerical model

Qiang Du*, Kai Tang, Calin D. Marioara, Sigmund J. Andersen, SINTEF Materials and Chemistry, Trondheim, Norway

Bjørn Holmedal, Randi Holmestad, Norwegian University of Science and Technology, Trondheim, Norway

*corresponding author: qiang.du@sintef.no

Abstract

The formation of the equilibrium precipitation phase during ageing treatment of Al-Mg-Si alloys is preceded by a series of metastable phases. Given inappropriate ageing time, higher ageing temperature or elevated temperature service condition, β'', the main hardening phase, would be replaced by the more stable metastable phases such as β', B', U1 and U2. The post-β'' microstructure evolution, called "over-ageing", leads to a steep drop in the hardness evolution curve. This paper aims to predict directly over-ageing in Al-Mg-Si alloys by extending a CALPHAD-coupled Kampmann-Wagner Numerical framework towards handling the coexistence of several types of stoichiometric particles of different phases. We demonstrate how the proposed modeling framework, calibrated with a limited amount of experimental measurement data, can aid in understanding the precipitation kinetics of a mix of different types particles. Simulation results will be presented for some earlier reported transmission electron microscopy measurements [1] to shed light on how the alloy composition and ageing treatment influence the post- β'' phase selection.

1. Introduction

The precipitation kinetics in heat-treatable aluminum alloys is quite complex. The formation of the equilibrium precipitate phase is preceded by a series of metastable ones due to their ease of nucleation. Examples include the needle β'' precipitate in Al-Mg-Si [2], the plate θ' precipitate in Al-Cu [3], the platelet η' precipitate in Al-Zn-Mg [4], and the lath S' precipitate in Al-Cu-Mg alloys [5]. It is these metastable precipitates rather than their stable counterparts that are contributing to peak hardening. However, given longer ageing time, higher ageing temperature or extended service time at an elevated temperature the precipitates responsible for the peak hardness will be replaced by other more stable precipitates, and eventually the equilibrium phases will form. This phenomenon is termed "over-ageing". During over-aging the precipitate density will decrease and the precipitate size will increase. Since a majority of the precipitates are non-

shearable, i.e. as strong pinning points as possible, the material strength will decrease as it becomes fewer of them [6].

There is a considerable industrial and academic interest in understanding the details of the transition from metastable to stable phases, especially concerning the industrially important Al-Mg-Si alloys. It has been established from Transmission Electron Microscopy (TEM) and High Resolution (HR) TEM investigations [2, 7] that the precipitation sequence from the quenched supersaturated solid solution (SSSS) at room temperature up to the formation of thermodynamically stable Mg_2Si (β) for most common Al-Mg-Si alloys is:

$SSSS \rightarrow Clusters \rightarrow Co-custers, GP(Mg_4AlSi_6) \rightarrow \beta''(Mg_5Si_6) \rightarrow \beta'(Mg_9Si_5), B'(Mg_9Al_3Si_7), U1(MgAl_2Si_2), U2(MgAlSi) \rightarrow \beta (Mg_2Si)$.

It should be noted that although the precipitate structures have been identified experimentally, the mixing of minor alloying elements and impurities (such as Cu) can alter their compositions, incite other precipitate structures or cause disorder, in addition to effects from the thermomechanical conditions and major alloy compositions. For example, β'' as well as β' precipitates can be disordered, containing regions of each other's structure and the U2 structures in the same needle [8]. In this paper we neglect such complications, and use the published compositions as the focus is on modeling the post-β'' transformation, i.e., how the β'' particles dissolve and post-β'' particles grow in an over-ageing condition. As discussed in [9], in Al-Mg-Si alloys the fully coherent monoclinic needle-shaped β'' phase, which dominates at peak hardness, is replaced by four less coherent (but still needle-shaped) phases during over-ageing: these are the hexagonal β', the trigonal U1 (TYPE-A), the orthorhombic U2 (TYPE-B) and the hexagonal B' (TYPE-C) which mostly nucleate on dislocations. Please note that instead of Type A, B and C as introduced by Matsuda et al [10], we use U1, U2 and B' as the notation in this paper. The main equilibrium phase is the cubic β, but the Si phase may also form. Whether a particular phase forms, depends on the ratio between Mg and Si in the chemical composition of the alloy, the ageing temperature and the thermo-mechanical processing history prior to the ageing treatment as revealed by the reported TEM characterizations [1]. For instance, Si-rich alloys tend to form U1, B' and Si particles during prolonged over-ageing, while Mg-rich alloys gain larger fractions of β' and U2. As earlier found, an alloy tends to mainly select a post-β'' phase having the Si/Mg ratio closest to its own Si/Mg ratio [1]. Due to the complex interactions among the many factors involved, it is desirable to have a model to predict directly this complex post-β'' microstructure evolution.

The development of such a predictive model requires understanding of the physical mechanisms behind the post-β'' transformations. In contrast to the pre-$\beta'' \rightarrow \beta''$ transformation, which is mainly achieved by changing the preceding phase composition, with minimal structural modifications [7], the $\beta'' \rightarrow$ post-β'' transformation must involve the dissolution of most of the β'' particles to provide solute for the growth of the new, and probably separate nucleation of β', B' or U phase particles, as the number densities of post-β'' phase particles are much less (about 1/1000 to 1/10) than the ones of β'' [1, 6]. In other words, the post-β'' transformation clearly requires diffusional transportation of solute between the dissolving and growing particles. It differs from the classical particle coarsening, i.e., Ostwald ripening, only in the origin of the thermodynamic driving force. The driving force for Ostwald ripening is interfacial energy, while the main driving force for the post-β'' transformation is the Gibbs energy difference between the dissolving (metastable) and growing (more-stable or stable) phases. This observation indicates that the post-β'' transformation could be modeled by extending the approach employed to model Ostwald ripening. The idea of transformation from GPI to GPII zones (metastable phases) via coarsening in Al-Cu alloys has already been suggested some years ago [11, 12]. In this paper this interesting topic is further explored to demonstrate how a coarsening model could be extended to simulate over-ageing in Al-Mg-Si alloys.

Many approaches, including the phase field method and the Kampmann-Wagner Numerical (KWN) approach, have been proposed in the literature for modeling coarsening. In contrast with the accurate but computationally expensive phase field approach [13], the KWN approach has been gaining popularity [14-26] recently. This is due to its mathematical simplicity and convenient coupling with the CALPHAD database, enabling an efficient treatment of multi-scale, multi-component industrially significant problems [14-25]. It should be noted that the coupling of the KWN model with the thermodynamic databases developed in the CALPHAD research community is a scale-bridging feature as the databases could be established on the base of first principle calculations [27, 28]. It has been pointed out by Kozeschnik et al that the coupling with the CALPHAD could bring the KWN approach's predictive power to a tuning parameter free level [29]. The KWN approach fits into our research purpose; therefore it is chosen to treat the post-β'' microstructure evolution.

The methodology of the KWN approach, initially proposed by Kampmann and Wagner in [19] for modeling precipitation kinetics, is also found in the seminal work of Maxwell and Hellawell published earlier, i.e. in 1975 on as-cast grain size prediction [26]. The essence of this approach is that the precipitate size distribution curve could be subdivided into size classes, each of which is associated with a number of identical precipitates. The temporal evolution of the size distribution is then tracked by following the size evolution of each discrete size class. This

modeling framework and its CALPHAD-coupled multi-component extensions have been seen as a key microstructure chain model in an Integrated Computational Materials Engineering (ICME) modeling framework to optimize alloy chemistry and heat treatment parameters for many industrial metallic materials [14-26]. In the most recent extension of the KWN approach, the assumption of the precipitate particles being spherical has been released enabling a better treatment of needle-shaped particles' precipitation kinetics in aluminum alloys [30, 31]. Another extension is reported in [32], where the KWN model is extended to accommodate the dislocation generation, the cluster formation and the competitive nucleation of β'' and β' precipitates during cold deformation, natural ageing and artificial ageing of aluminum alloys, respectively. All of these works reveal the versatile and generic nature of the KWN modeling framework. It should also be mentioned that rapid progress in the CALPHAD community on thermodynamic databases for metastable and stable phases, i.e. the work reported in [27, 28] on Al-Mg-Si alloy system, enables the applications of the KWN model to industrial alloys.

In this paper, we will extend the multi-component KWN model reported in [16, 30, 31] to treat concurrent nucleation, growth and coarsening of multi-phase precipitate particles. The coupling of the extended model with the reported CALPHAD databases [27, 28] will be implemented. Then the new model will be applied to predict the post-β'' microstructural evolution during over-ageing of Al-Mg-Si alloys. The simulations will be discussed together with some reported TEM measurement to shed light on how the alloy composition and ageing temperature influence the post-β'' phase selection.

2. Model Description

In this section the assumptions in deriving the multi-phase KWN model is listed and the adaptions to the KWN model toward the multi-phase extension are described.

2.1 The assumptions

Our idea is to consider the post-β'' transformation as Ostwald ripening driven by the Gibbs energy difference between the dissolving (metastable) and growing (more-stable or stable) phases instead of interfacial energy. Using the CALPHAD-coupled multi-component version of the KWN model reported in [16, 30, 31] as a starting point, the extension required to treat concurrent nucleation, growth and coarsening of multi-phase particles is adding one more interfacial phase composition relation equation for each extra precipitation phase. Before proceeding to the multi-phase KWN model description, it is useful to summarize the assumptions adopted below.

For the calculation of precipitate growth rate, the assumptions include:

- The precipitate shape is assumed to be represented by an elongated sphere, i.e., a prolate with a constant aspect ratio.
- Precipitate growth/dissolution is solely controlled by diffusion in the matrix.
- The invariant field assumption is employed in computing the diffusion field surrounding each growing precipitate.
- Depending on the magnitude of its diffusivity, the diffusion of an alloying element inside a precipitate could be modeled either with an infinitely high (uniform compositional profile across the precipitate) or with no solute diffusion in the precipitate (freezing compositional profile across the precipitate).
- Local equilibrium modified by the Gibbs-Thomson effect prevails at various precipitate-matrix interfaces.
- The molar volumes of the matrix and precipitate phases are identical.

For precipitate nucleation the classical phenomenological heterogeneous nucleation law is adopted, and the nucleation rate could be calculated by:

$$\frac{dN}{dt} = (N_0 - N_{tot}^{\beta}) Z \beta^* \exp(-\frac{\Delta G^* f(\theta)}{kT}) \exp(-\frac{\tau}{t}) \qquad (1)$$

Where Z is the Zeldovich factor with $Z = \frac{v_{at}^P}{2\pi R^*} \sqrt{\frac{\gamma}{k_B T}}$. β^* is the condensation rate of solute

atoms in a cluster of critical size with $\beta^* = \frac{4\pi R^{*2} DX}{a^4}$. $R_{k_B T}^*$ is the nucleus size with

$R_{k_B T}^* = R^* + \frac{1}{2}\sqrt{\frac{k_B T}{\pi \gamma}}$. ΔG^* is the energy required to form a critical nucleus of radius R^* with

$\Delta G^* = \frac{16\pi \gamma^3}{3\Delta G_v^2}$. $f(\theta)$ is the geometrical factor with $f(\theta) = (1/2)(2 + \cos\theta)(1 - \cos\theta)^2$. τ is the

incubation time for nucleation with $\tau = \frac{2}{\pi \beta^* Z^2}$. The physical properties required in Eq.(1) are

N_0, the number of heterogeneous nucleation sites per unit volume, γ, the interfacial energy, D, the diffusivity of an alloying component in the matrix, ΔG_v, the driving force for precipitation per unit volume, X the matrix mean solute atom fraction, v_{at}^P is the mean atomic volume within precipitates and a the lattice parameter of the matrix phase. N_{tot}^{β} is the actual total density of nucleated precipitates. θ is the wetting angle of the β phase with its heterogeneous nucleation site. It should be noted that the nucleation model input parameters such as N_0 and γ have to be

tuned with the experimental measurement data. The tuning of these parameters in our simulations is described in Section 3.2.

2.1 Solute conservation and growth rate calculation

Considering the precipitation of spheroid secondary phase particles from a solid solution α matrix phase with its volume denoted by V_{Domain} and nominal composition by c_i^0, the following equation could be written for the alloying component i according to the solute balance equation:

$$\sum_{k=1}^{NOP}\sum_{j=1}^{NOS}\frac{4}{3}\pi R_{j,k}^3 n_{j,k} c_{j,i,k}^\beta + (V_{Domain} - \sum_{j=1}^{NOP}\frac{4}{3}\pi R_j^3 n_j)c_i^\alpha = V_{Domain} c_i^0 \tag{2}$$

Here R_j, $c_{j,i}^\beta$, and n_j are the volume-equivalent spherical particle radius, average composition, and number of the precipitates associated with size class j, respectively. The total number of size classes and precipitating phases are denoted as *NOS* and *NOP,* respectively. c_i^α is the average composition of element i in the matrix.

The compositional profile of component i across a precipitate could be approximated as either "uniform" (infinite diffusion) or "freezing" (no diffusion). In the two scenarios, $c_{j,i}^\beta$ can be related to the interfacial precipitate phase composition via one of the following equations (please note the subscript k is omitted here):

$$c_{j,i}^\beta = c_{j,i}^{\beta\,*}, \ \text{ infinite diffusion} \tag{3}$$

$$c_{j,i}^\beta(R_j) = \frac{\int_0^{R_j} c_{j,i}^{\beta\,*}(r)4\pi r^2 dr}{4\pi R_j^3/3} = \frac{3\int_0^{R_j} c_{j,i}^{\beta\,*}(r)r^2 dr}{R_j^3}, \ \text{ no diffusion} \tag{4}$$

Here $c_{j,i}^{\beta\,*}$ is used to denote the interfacial composition of one of the precipitating phases associated with size class j.

The key in the KWN modeling framework is to calculate the evolution of the volume equivalent spherical particle radius for each size class. Based on the assumptions listed above and the correction factor f introduced in [30, 31], the changing rate of the equivalent radius could be calculated from the diffusion of alloying component i:

$$\dot{R}_j = f\frac{D_i(T)}{R_j}\frac{c_i^\alpha - c_{j,i}^{\alpha*}}{c_{j,i}^{\beta\,*} - c_{j,i}^{\alpha*}} = f\frac{D_i(T)}{R_j}\frac{\Delta c_{j,i}^\alpha}{\Delta c_{j,i}^{\beta/\alpha}} \tag{5}$$

In which the correction factor f is defined as:

$$f(\alpha) = \frac{2\sqrt{\alpha^2-1}}{\sqrt[3]{\alpha}\ln\left(2\alpha^2+2\alpha\sqrt{\alpha^2-1}-1\right)}$$

(6)

For the special limit of spheres, i.e. with $\alpha = 1$, the shape factor $f(\alpha)$ degenerates smoothly to $f(1) = 1$, i.e. the spherical shape growth rate equation. In general in multi-component systems, multiple growth rate equations are applied, and it is convenient to organize Eq.(5) in the following general form:

$$\dot{R}_j = f(\alpha)\frac{D_i(T)}{R_j}\frac{\Delta c_{j,1}^{\alpha}}{\Delta c_{j,1}^{\beta/\alpha}}$$

(7)

$$D_i\frac{\Delta c_{j,i}^{\alpha}}{\Delta c_{j,i}^{\beta/\alpha}} = D_1\frac{\Delta c_{j,1}^{\alpha}}{\Delta c_{j,1}^{\beta/\alpha}} \text{ for i} \geq 2$$

(8)

Here Eq.(7) is called the growth rate equation and Eq.(8) the growth rate constraint equation. As to be discussed in the next subsection, Eq.(8) together with local equilibrium assumption determines interfacial phase compositions.

2.2 Interfacial phase compositions

The interfacial phase compositions, $X_{j,i}^{*\alpha}$ and $X_{j,i}^{*\beta}$, enter the growth rate equations, i.e., Eq.(5). Their values are calculated by the assumption of local equilibrium (modified by the Gibbs-Thomson effect) at the matrix-precipitate interface and Eq.(8) [16]. Following our previous work, the equations held at each precipitate-matrix interface in the original KWN model [16] are modified into:

$$T = T^{\alpha}\left(c_{j,i}^{\alpha*}, \frac{R_j}{g(\beta)}\right)$$

(9)

$$c_{j,i}^{\beta*} = \frac{c_{j,i}^{\alpha*}}{k_i\left(c_{j,i}^{\alpha*}, \frac{R_j}{g(\beta)}\right)}$$

(10)

Where T^{α} represents the solvus temperature hyper-surface and k_i the partition coefficient of alloying element i of a Gibbs-Thomson phase diagram. The correction factor, g, a modification of

the volume-equivalent spherical particle curvature $1/R$ to account for the energetic cost of creating new non-spherical particle interface, is

$$g(\alpha) = \left(1 + \frac{\alpha}{\sqrt{1 - \frac{1}{\alpha^2}}} \sin^{-1} \sqrt{1 - \frac{1}{\alpha^2}}\right) \frac{1}{2\alpha^{2/3}} \qquad (11)$$

2.3 The thermodynamic description of the metastable phases in the Al-Mg-Si alloys

Thermodynamic descriptions of the stable and metastable phases in the Al-Mg-Si ternary system have been reported by a number of authors [27, 28, 33-35]. The early assessment reported by Feufel et al. was used to construct the well-known COST507 light metal database [33]. The later assessment by Zhang et al. [27] was actually based on the COST507 database by adding the metastable phases, β'-$Mg_{18}Si_{10}$ and β''-Mg_5Si_6. Thermodynamic properties of these metastable phases were calculated using first-principles simulations. Povoden-Karadeniz et al. [28] proposed another set of metastable phases, namely Mg_5Si_6 (β''), $Mg_{1.8}Si$ (β'), $Al_3Mg_9Si_7$/$Al_3Mg_8Si_7$ (B'), Al_2MgSi_2 (U_1) and $MgAlSi$(U_2). They also proposed a five sub-lattice formalism: $(Al,Si)_{1/4}(Al,Si)_{1/4}(Al,Si)_{1/4}(Al,Si)_{1/4}Va$, for the description of the metastable GP-zone. Thermodynamic properties of the metastable phases as well as the end-members of the non-equilibrium solutions were determined using the Vienna Ab initio Simulation Package (VASP). The metastable phases were also modelled by Harvey in 2006 and were later implemented to the FTLite database in the FactSage software package [35]. However, the assessment has not been published yet. The metastable phases, β''-Mg_5Si_6, β'-Mg_9Si_5, B'-$Mg_9Si_7Al_3(Al,Mg,Si,Va)_2$, U1-$Al_2MgSi_2$ and U2-$Mg_4Al_4Al_2(Al,Si)_2$ were modelled by Harvey, in which also the pre-β'' and β'' were modelled as non-equilibrium solution phases.

The following metastable phases have been used in the present simulations: β''-Mg_5Si_6, β'-Mg_9Si_5, B'-$Mg_9Si_7Al_3(Al,Mg,Si,Va)_2$, U_1-Al_2MgSi_2 and U_2-$Mg_4Al_4Al_2(Al,Si)_2$. The metastable β' and β'', represented by Mg_5Si_6 and Mg_9Si_5, were taken from the FTLite database. B', U_1 and U_2, represented by $Mg_9Al_3Si_7$, $MgAl_2Si_2$ and $MgAlSi$, respectively, were taken from Povoden-Karadeniz et al. [28]. The thermodynamic descriptions of the stable phases in the Al-Mg-Si system were taken from the COST507 database. Fig. 1 shows the solvus boundaries in the isopleth of 0.76 at% Si calculated using the database used in our simulations, where the experimental data were reproduced from the diagram reported by Zhang et al. [27] and are represented with the markers (circles for fcc+ β'' phase region and triangle for fcc+ β' phase region). Reasonable agreement between the database calculation and the experimental measurement has been obtained, confirming the quality of the database.

Al - Mg - Si
Si mole fraction at 0.0076

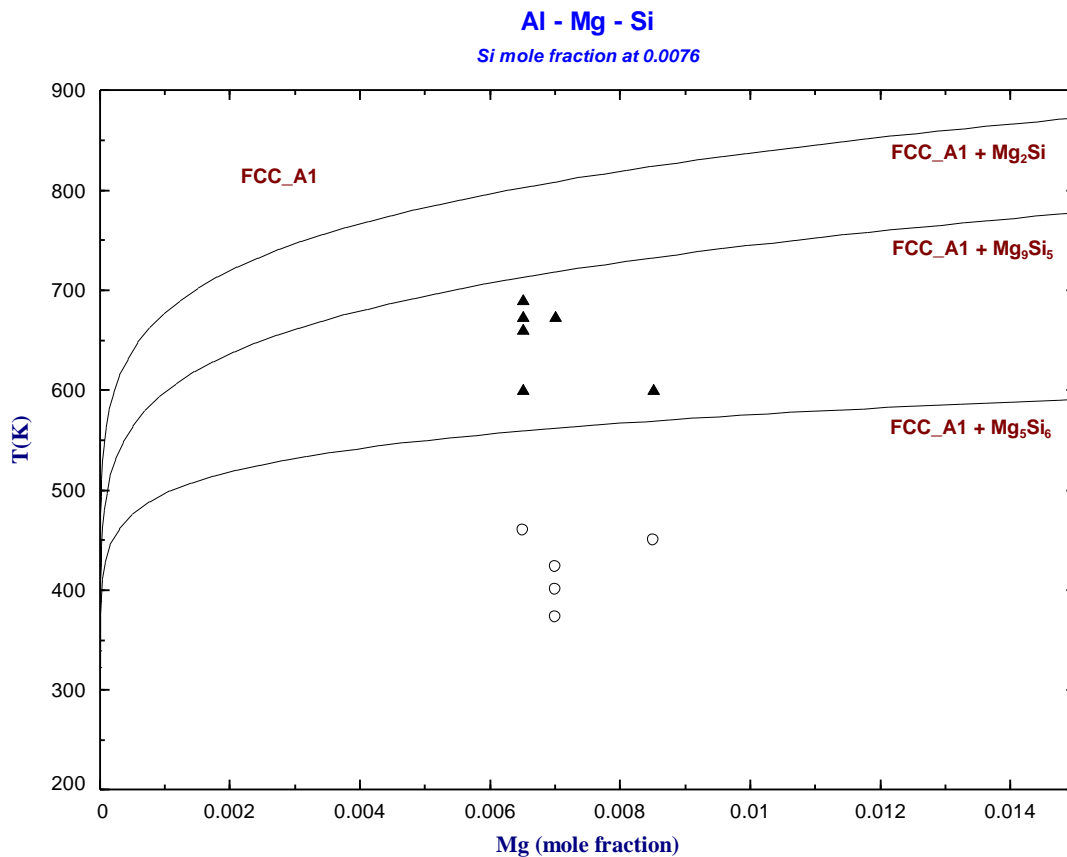FCC_A1

FCC_A1 + Mg₂Si

FCC_A1 + Mg₉Si₅

FCC_A1 + Mg₅Si₆

Fig. 1 Solvus boundaries in the isopleth of 0.76 at% Si calculated using the COST507 database and metastable phases reported in the FTLite databases with the data points in [27].

3. Results and Discussion

3.1 Experimental data

Two Al-Mg-Si alloys that had earlier been studied in [1], are considered. Following the notation in [1], they are labelled as A3 and A12 with compositions (in atomic percent) of Al-0.58Mg-0.72Si and Al-0.72Mg-0.57Si, respectively. Two heat treatments were performed as reported in [1]. The first one, labelled H1, consisted of a 2 hours solution heat treatment at 570 °C, water-quench to room temperature (RT) and four hours RT-storage before ageing. The H1 samples were next quickly heated to 250 °C and aged in steps from 10 min to 8 hours. After ageing the samples were cooled in water. The second heat treatment, labelled H2, consisted of 1 hour solution heat-treatment at 540 °C, water-quench to RT and 4 hours storage at RT prior to a two-step ageing treatment. Firstly the material was kept 17 hours at 175 °C, providing a nearly peak hardened condition, containing a high density of fine β'' needles. Consequently, a quick heating to 260 °C was followed by further aging between 10 minutes and 5 hours.

TEM measurements of precipitate number densities and distributions of their phases were performed in [1] subsequent to 10 min and 3 hours aging in the H1 and (second part) H2 heat treatments. These results are here re-listed in Table 1 and 2.

Table 1 Experimental measurements on samples aged for 10 minutes and 3 hours: particle number densities

Heat treatment	A3 (#/μm³)	A12 (#/μm³)
H1, 10 minutes aging	4241±249	2651±201
H2, 10 minutes aging	5227±191	2271±75
H1, 3 h aging	348.5±31	176.5±8
H2, 3h aging	272.5±13	139.3±8

Table 2 Experimental measurements on samples aged for 3 hours: distributions of phases, scaled to 100%

Phase	A3/H1 (%)	A3/H2 (%)	A12/H1 (%)	A12/H2 (%)
β''(Mg_5Si_6)	0	0	0	0
β'(Mg_9Si_5)	26	6	96	97
B'($Mg_9Al_3Si_7$)	4.5	6	0	0
U1($MgAl_2Si_2$)	4.5	16	4	7
U2($MgAlSi$)	65	72	0	3
β (Mg_2Si)	0	0	0	0

3.2 Model calibration

One of the key thermo-physical input parameters to the model is the interfacial energy γ, which influences both of nucleation rate and coarsening rate. It is very difficult to pin down its value accurately. Based on a literature survey [20, 21, 36, 37], for β'' and β phases the interfacial energy ranges from 0.08 to 0.25 J/m², while no data could be found for the U1, U2, β' and B' phases. Kozeschnik et al. [29] has pointed out that the interfacial energies can be evaluated based on the solution enthalpy of the precipitation phase. Following their idea, and with the input of their Al-Mg-Si thermodynamic database [29], the interfacial energy values have been calculated in Table 3 for all the involved metastable phases. The interfacial energies applied in

our current simulations, as listed in Table 3, are based on calibration to the experimental data reported in Table 1. They are within the reported range and do not deviate much from the calculated values using Kozeschnik's solution enthalpy method.

Table 3 Interfacial energies used in the simulations and calculated using Kozeschnik's solution enthalpy method

Interface	Used in the simulation	Calculated using Kozeschnik's solution enthalpy, averaging in {100}, {111} and {110} planes
β'' and FCC phases	0.084	0.157
β' and FCC phases	0.18	0.198
U1 and FCC phases	0.18	0.112
U2 and FCC phases	0.18	0.121
B' and FCC phases	0.18	0.151
β and FCC phases	0.20	0.227

The classical heterogeneous nucleation model was employed to describe the competitive nucleation of the metastable β'', β', U1, U2, B' and β phases. An important input parameter to the nucleation model is the number of heterogeneous nucleation sites N_0. Firstly, this parameter was estimated basing on the measured particle number densities shown in Table 1 by assuming that the measured number densities from samples after 10 minutes ageing treatment correspond to the total number of heterogeneous nucleation sites available for all type of precipitates. Furthermore, the number density measured from the 3 hours samples are assumed to correspond to the number of post-β'' particles nucleation sites. The fraction of each type of post-β'' nucleation type of sites, amongst β', B', U1, U2 and β phases, are assumed to be the same as the measured phase distributions listed in Table 2. With all these assumptions, the number of heterogeneous nucleation sites for each type of particle used in the simulations are derived and listed in Table 4. It should be noted that the assumptions only specify a maximum particle number density for each phase, and does not constrain their evolution paths while the proposed model is able to make such a prediction. Other model input parameters are estimated based on the literature and are listed in Table 5. It should be mentioned that for simplicity the precipitate particle's aspect ratio is assumed to be 1, i.e., spherical shape although the proposed model is capable of handling non-spherical particles.

Table 4 The number of heterogeneous nucleation sites for each type of particle used in the simulations

	A3/H1 (#/μm³)	A3/H2 (#/μm³)	A12/H1 (#/μm³)	A12/H2 (#/μm³)
$\beta''(Mg_5Si_6)$	4000	5200	2700	2271
$\beta'(Mg_9Si_5)$	100	53	200	140
$B'(Mg_9Al_3Si_7)$	0	25	0	0
$U1(MgAl_2Si_2)$	20	250	10	0
$U2(MgAlSi)$	200	250	0	10
$\beta\ (Mg_2Si)$	0	0	0	0

Table 5 Other material property and nucleation input parameters used in the simulations

Molar volume of β'', β' and FCC phases	1.0×10^{-5} m3/mol		
Lattice parameters in FCC phase	0.404 nm		
Diffusivities in the FCC phase [38]		Diffusion constant (m2/s)	activation energy (kJ/mole)
	Mg	1.49×10^{-5}	120.5
	Si	1.38×10^{-5}	117.6
Gibbs-Thomson phase diagram	Metastable phase diagram generated by first principle calculations in [28].		
Precipitate particle's aspect ratio	1.0		

3.3 Model predictions

Being calibrated by the limited amount of experimental measurement data (as illustrated in Section 3.2), the proposed model was applied to predict the full microstructure evolution paths during the two ageing treatments, i.e., H1 and H2, of the A3 and A12 alloys.

Among the four simulations results the one for the A12/H1 condition are used to illustrate the microstructure evolution. It starts with nucleation events. According to the adopted first-principle based thermodynamic descriptions of the precipitating phases, β', B', U1, U2 and β have a larger volumetric nucleation driving force than β''. According to the model calculation the nucleation driving force for the precipitation of β' and β'' are 11.5 and 3.4 kJ/mol, respectively.

Although the β' phase has a higher driving force, this does not give it a lead in nucleation owing to its larger interfacial energy value (0.18 vs. 0.084 J/m² as shown in Table 3). The calculated critical nucleation driving forces for the two phases are comparable, leading to the same duration to reach their peak particle number density as shown in Fig. 2. Please note that the nucleation model adopted here is of phenomenological nature, and does not capture the complex nucleation mechanisms revealed by the detailed TEM studies. Nevertheless this treatment is considered as sufficient for the investigation in this paper as the aim of this paper is to model the competitive growth and coarsening of the metastable and stable precipitating phases.

Fig. 2 shows that after about 0.1 hour of ageing treatment, nucleation ceases due to the exhaustion of heterogeneous nucleation sites. The predicted maximum number density of β'' precipitates is much higher than (about 13 times) the one of β'. After a short plateau with the duration of 0.8 hours the predicted β'' number density decreases and approaches rapidly to zero. Meanwhile the number density of β' precipitates remains constant.
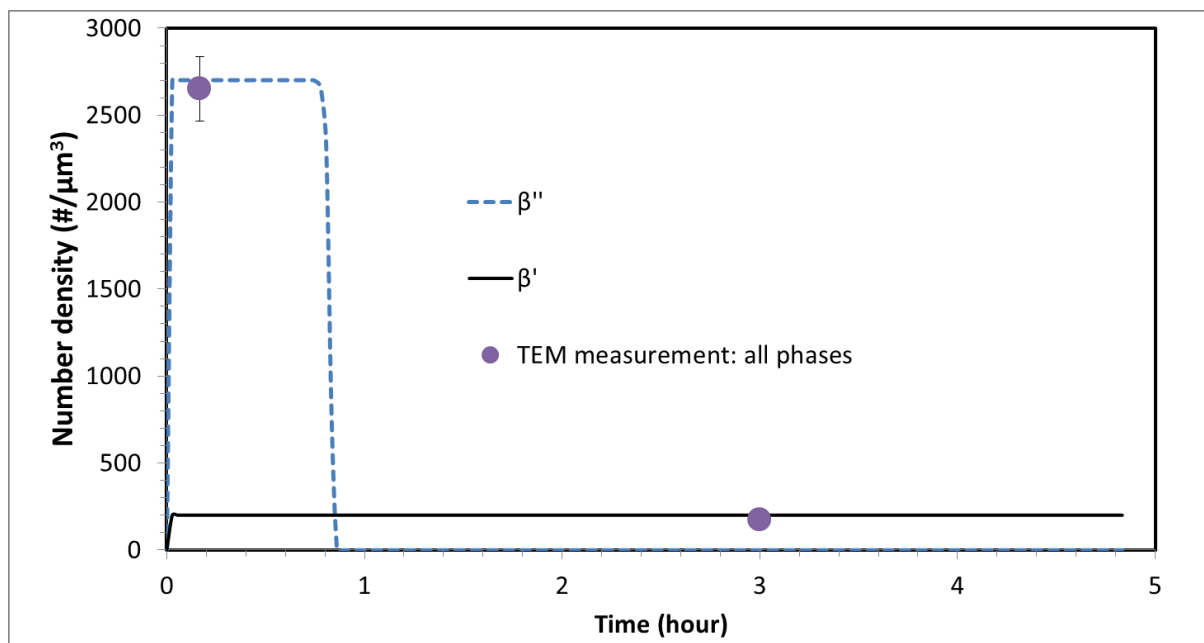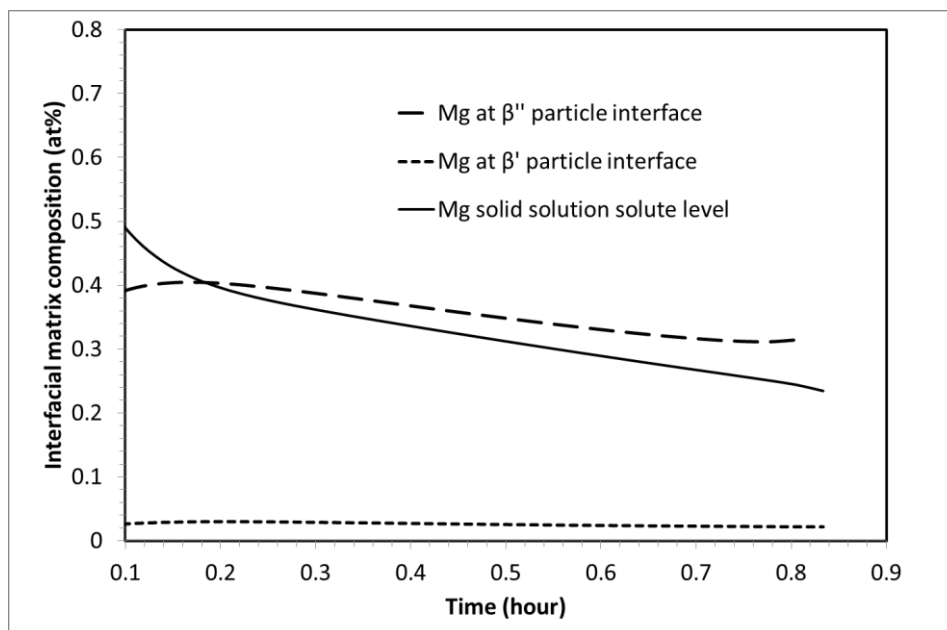

Fig. 2 The evolution of β'' and β' particles number density for the A12 alloy aged under H1 heat treatment, i.e., with a constant ageing temperature of 250 °C.

Fig. 3 and 4 illustrate how growth and coarsening mechanisms operate in the post-β'' transformation, i.e., within the duration between 0.1 hour and 0.9 hour ageing treatment. Fig. 3 shows the predicted evolution of interfacial matrix phase compositions at a growing β'' and β' particle together with solid solution levels. Initially the Mg and Si solid solution solute levels are higher than the ones at the interfacial matrix phase for both of the β'' and β' particles. It allows

transfer of solutes by diffusion to the matrix-precipitate interface and both of the β'' and β' particles are able to grow. One also should notice that the interfacial matrix compositions at the growing β'' particle front are higher than the ones at β' particle giving the former particle disadvantage in the competition for the solutes. However, this disadvantage does not lead to dissolution of β'' particles until when the β'' particle interfacial compositions are below the solid solution level, i.e. at the ageing time of 0.18 hour. After this point, solutes only diffuse towards the β' growing fronts, while they are diffused away from the β'' fronts. Consequently β'' particles shrink as seen in Fig. 4, where their volume fraction evolution curve is plotted. All β'' particles are dissolved at the ageing time of 0.9 hour, while β' particles keep growing until 2 hour of ageing time (Fig. 4), from which their final fraction stays at 1.1% (Fig. 4).

Fig. 4 shows the model prediction of the evolution of particles volume fraction. It is plotted together with two experimental measured data points. The model prediction reveals that there is an abrupt change in precipitates volume fraction after about 1 hour of ageing treatment. As shown in Fig. 4, this change corresponds to the dissolution of β'' particles and rapid growth of β' particles. Having a much lower phase fraction at the initial stage of ageing treatment than β'', the β' phase continuously grows at the cost of β'' phase. The β'' phase fraction attains a maximum (0.5%) after 0.1 hours ageing treatment, while it gradually decreases to zero and the β' phase fraction increases to 1.1%. The particle volume fraction in Fig. 4 agrees reasonable with experimental points, considering the error in the experimental measurement and the few calibration parameters in the simulation.

(a) Mg
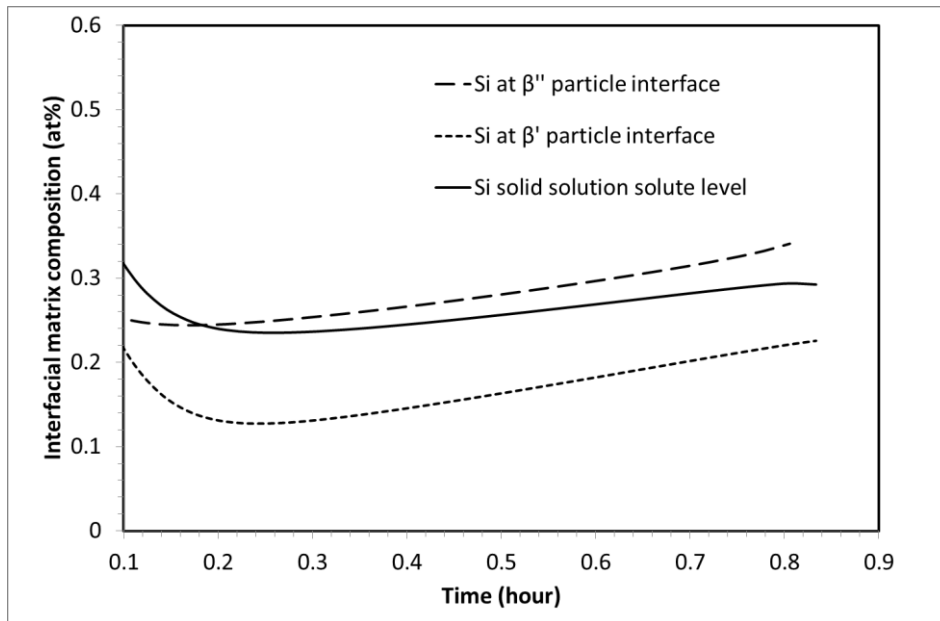
(b)

Fig.3 Predicted evolutions of interfacial solute concentrations at two selected growing β'' and β' particles and the corresponding solid solution solute level for a) Mg, b) Si, for the A12 alloy aged under H1 heat treatment, i.e. with a constant ageing temperature of 250 °C
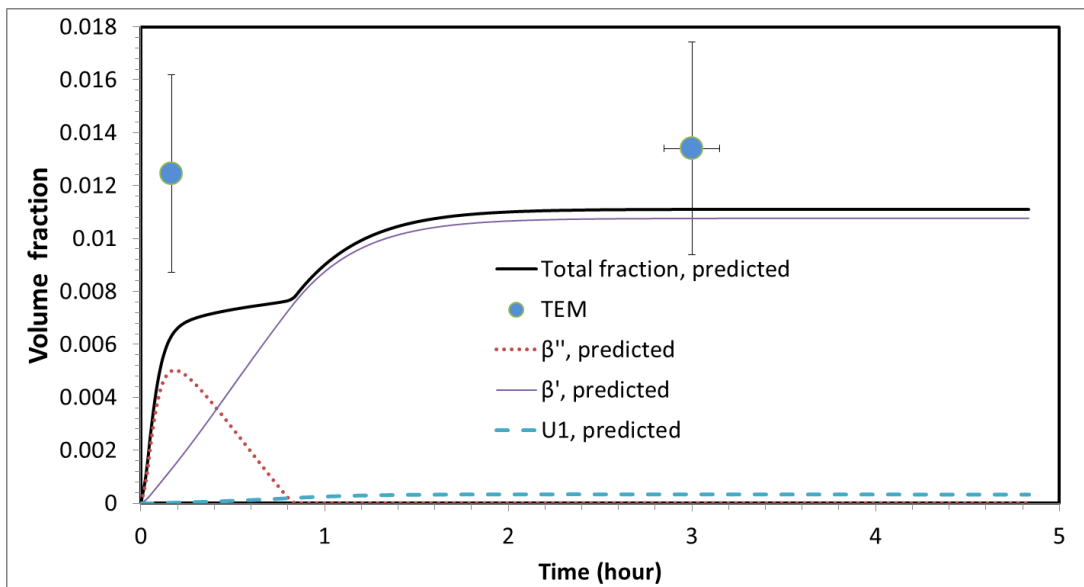

Fig. 4 The evolution of the precipitating phase's volume fractions for the A12 alloy aged under the H1 heat treatment, i.e. with a constant ageing temperature of 250 °C

In Fig. 5 the evolution of particle volume fractions are presented for the A12 alloy aged under the H2 heat treatment and the A3 alloy aged under the H1 heat treatment. It should be noted

that the abrupt increase in the aging temperature in the A12/H2 simulation instantly causes a subsequent dissolution of the β'' particles.
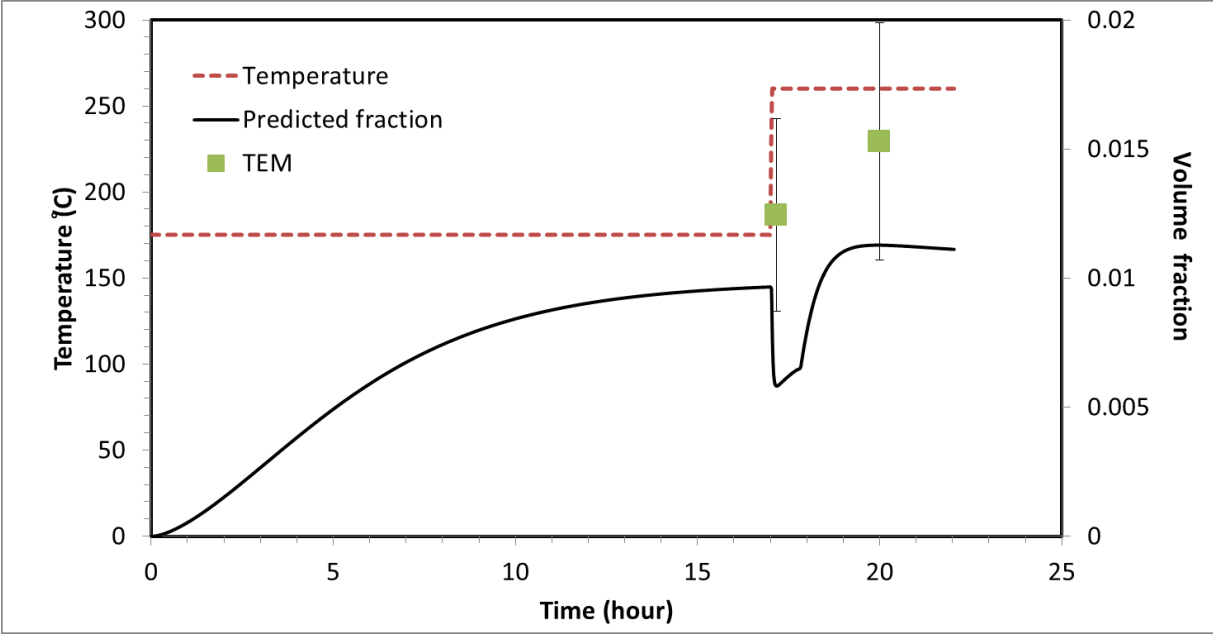
(a)
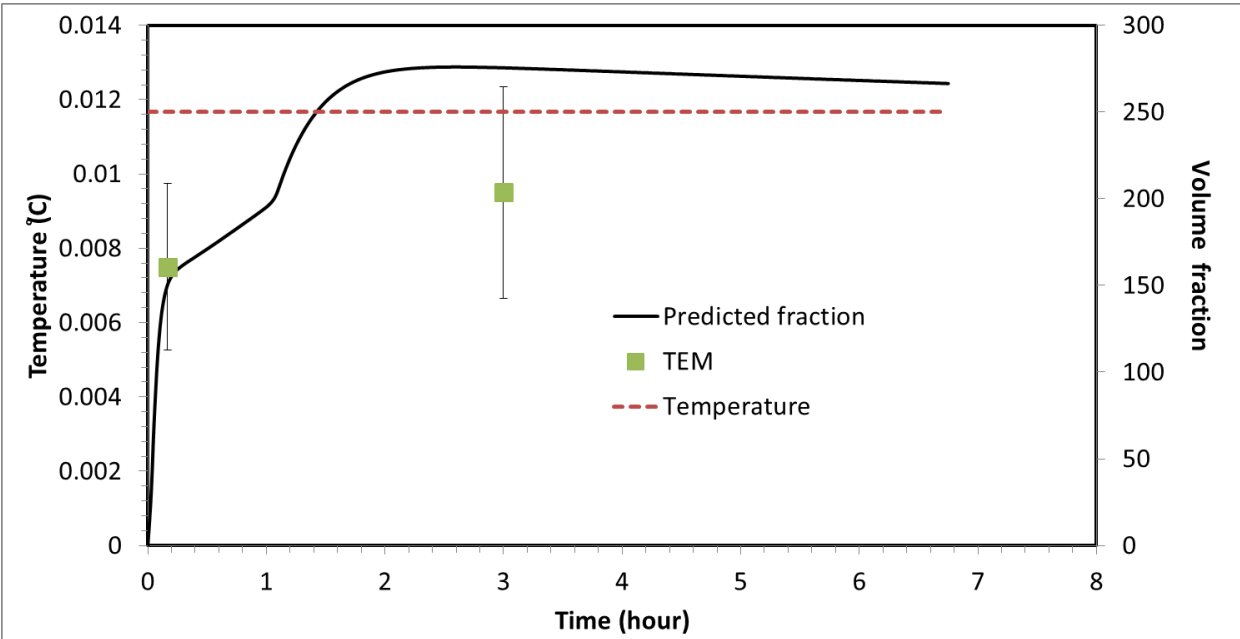
(b)

Fig. 5 The evolution of volume fraction for all precipitate phases in the A12 alloy aged under the H2 heat treatment condition (a) and the A3 alloy aged under the H1 heat treatment condition (b)

3.4 Discussion

The model could be employed to give a better understanding of post-β'' phase selections. Fig.6 shows the calculated nucleation driving forces for all the metastable phases under the two different heat treatment conditions. If we compare the Si rich A3 alloy with the Mg rich A12 alloy, the driving forces for the Mg richer metastable phases, β' and B' are larger in the Mg rich A12 alloys, while the driving forces in Si rich phases (U1 and U2) are larger in the Si rich alloys. It indicates that it is thermodynamically easier to nucleate the Mg richer phases in the Mg rich alloys. Even though the accuracy of the interfacial energies for the involved metastable phases should be improved to achieve better predictive power on nucleation, this observation qualitatively supports the conclusions drawn from TEM characterization by Marioara et al [1] that an alloy tends to select as main post-β'' phase the precipitate having the Si/Mg ratio closest to the alloy's own Si/Mg ratio.
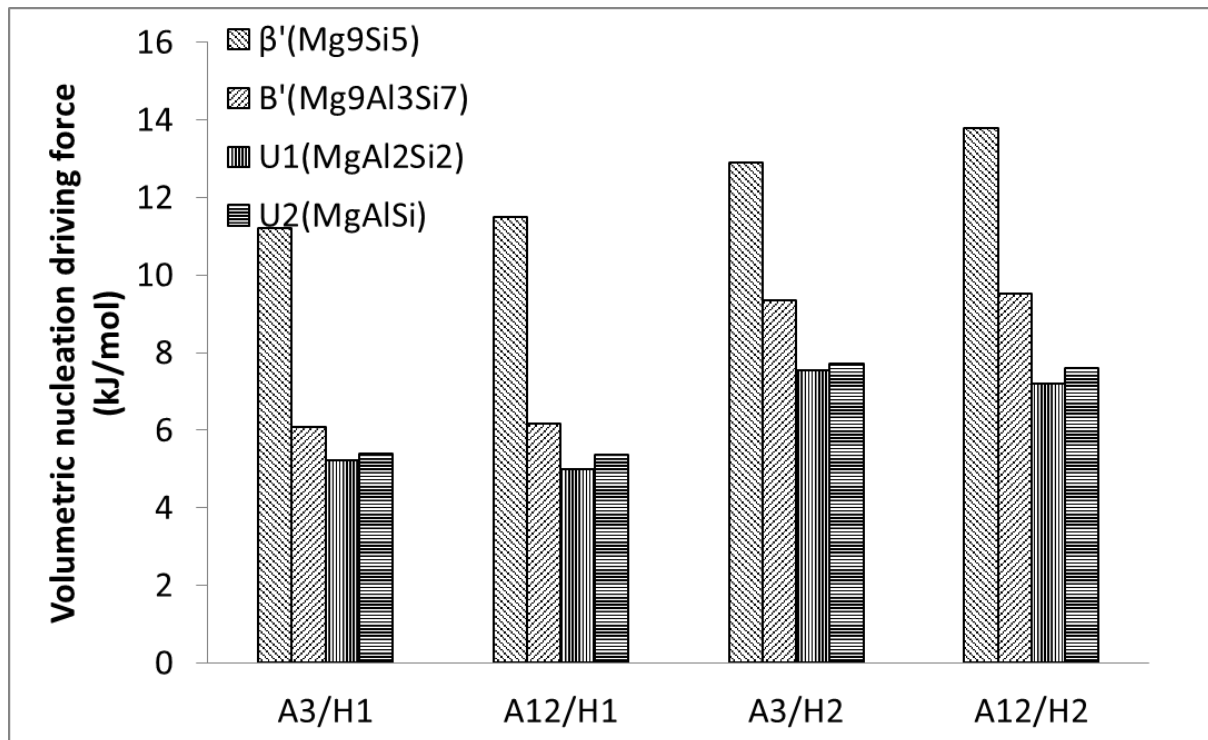

Fig. 6 The calculated volumetric nucleation driving force for the formation of post-β'' phases for the A3 and A12 alloys heat treated under H1 and H2 conditions.

The model is composition dependent owing to its coupling with the CALPHAD database, and could be used for other alloys or different heat treatment conditions. This has been demonstrated in Fig. 5 on the evolution of particles volume fraction for the A12 alloy aged under the H2 heat treatment condition and the A3 alloy aged under the H1 heat treatment condition. The model, being calibrated with only a few experimental data, is able to produce the whole microstructure evolution paths for different alloys.

Having demonstrated the proposed model predictive power, the performed simulations have also revealed the model's limitations. One of the limitations originates from the validity of the assumptions in calibrating the heterogeneous nucleation model. We have assumed that the experimentally measured number densities correspond to the number of heterogeneous nucleation sites. This is a rough estimation and has neglected the underlying complex nucleation mechanisms. While the calibrated numbers of the nucleation sites is not general, it does not hinder the model predictions on the post- β'' transformation, which is essentially in a coarsening stage. The tuning of the interfacial energies for the different metastable phases is also a subject to criticisms, and the first-principle based solution enthalpy method proposed by Kozeschnik et al [29] have shown some predictive powers in providing reasonable estimations.

4. Conclusions

A CALPHAD-coupled multi-component KWN model has been extended to simulate concurrent nucleation, growth and coarsening of multi precipitating phases. We have demonstrated that the model could be applied to predict over-ageing, i.e., growth of post-β'' metastable phases at the cost of the needle-shaped β'' phase and during extended ageing treatment of Al-Mg-Si alloys. The proposed modeling framework is able to shed light on how the alloy composition and ageing treatment influence the post- β'' phase selection. We also emphasize that the interfacial energies and the number of heterogeneous nucleation sites are critical input parameters for the numerical simulations.

5. Acknowledgements

6. Reference

[1]   Marioara CD, Nordmark H, Andersen SJ, Holmestad R. Post-β'' phases and their influence on microstructure and hardness in 6xxx Al-Mg-Si alloys. 2006 *Journal of Materials Science* 41(2):471-8.

[2]   Marioara CD, Andersen SJ, Jansen J, Zandbergen HW. The influence of temperature and storage time at RT on nucleation of the beta '' phase in a 6082 Al-Mg-Si alloy. 2003 *Acta Materialia* [Article] 51(3):789-96.

[3]   Biswas A, Siegel DJ, Wolverton C, Seidman DN. Precipitates in Al-Cu alloys revisited: Atom-probe tomographic experiments and first-principles calculations of compositional evolution and interfacial segregation. 2011 *Acta Materialia* 59(15):6187-204.

[4]   Sha G, Cerezo A. Early-stage precipitation in Al-Zn-Mg-Cu alloy (7050). 2004 *Acta Materialia* 52(15):4503-16.

[5]   Rometsch PA, Zhang Y, Knight S. Heat treatment of 7xxx series aluminium alloys-Some recent developments. 2014 *Transactions of Nonferrous Metals Society of China* 24(7):2003-17.

[6]   Marioara CD, Andersen SJ, Zandbergen HW, Holmestad R. The influence of alloy composition on precipitates of the Al-Mg-Si system. 2005 *Metallurgical and Materials Transactions a-Physical Metallurgy and Materials Science* [Article] 36A(3A):691-702.

[7]   Chen JH, Costan E, van Huis MA, Xu Q, Zandbergen HW. Atomic pillar-based nanoprecipitates strengthen AlMgSi alloys. 2006 *Science* 312(5772):416-9.

[8]   Andersen SJ, Marioara CD, Frøseth A, Vissers R, Zandbergen HW. Crystal structure of the orthorhombic U2-Al4Mg4Si4 precipitate in the Al–Mg–Si alloy system and its relation to the β′ and β″ phases. 2005 *Materials Science and Engineering: A* 390(1–2):127-38.

[9]   Wenner S, Nishimura K, Matsuda K, Matsuzaki T, Tomono D, Pratt FL, et al. Clustering and Vacancy Behavior in High- and Low-Solute Al-Mg-Si Alloys. 2014 *Metallurgical and Materials Transactions a-Physical Metallurgy and Materials Science* [Article] 45A(12):5777-81.

[10]   Matsuda K, Sakaguchi Y, Miyata Y, Uetani Y, Sato T, Kamio A, et al. Precipitation sequence of various kinds of metastable phases in Al-1.0mass% Mg2Si-0.4mass% Si alloy. 2000 *Journal of Materials Science* [Article] 35(1):179-89.

[11]   Matsubara E, Cohen JB. The G.P. zones in Al Cu alloys—I. 1985 *Acta Metall Mater* 33(11):1945-55.

[12]   Matsubara E, Cohen JB. The G.P. zones in Al Cu alloys—II. 1985 *Acta Metall Mater* 33(11):1957-69.

[13]   Chen L-Q. PHASE-FIELD MODELS FOR MICROSTRUCTURE EVOLUTION. 2002 *Annual Review of Materials Research* 32(1):113-40.

[14]   Myhr OR, Grong O. Modelling of non-isothermal transformations in alloys containing a particle distribution. 2000 *Acta Mater* 48(7):1605-15.

[15]   Du Q, Poole WJ, Wells MA, Parson NC. Microstructure evolution during homogenization of Al-Mn-Fe-Si alloys: Modeling and experimental results. 2013 *Acta Materialia* 61(13):4961-73.

[16]   Du Q, Poole WJ, Wells MA. A mathematical model coupled to CALPHAD to predict precipitation kinetics for multicomponent aluminum alloys. 2012 *Acta Materialia* 60(9):3830-9.

[17]   Robson JD, Jones MJ, Prangnell PB. Extension of the N-model to predict competing homogeneous and heterogeneous precipitation in Al-Sc alloys. 2003 *Acta Materialia* 51(5):1453-68.

[18]   Perez M, Dumont M, Acevedo-Reyes D. Implementation of classical nucleation and growth theories for precipitation. 2008 *Acta Materialia* [Article] 56(9):2119-32.

[19]   Wagner R, Kampmann R. Homogeneous second phase precipitation. In: Cahn RW, Haasen P, Kramer EJ, editors. Materials science and technology: a comprehensive treatment. Weinheim, Germany: VCH; 1991. p. 213-303.

[20]   Bardel D, Perez M, Nelias D, Deschamps A, Hutchinson CR, Maisonnette D, et al. Coupled precipitation and yield strength modelling for non-isothermal treatments of a 6061 aluminium alloy. 2014 *Acta Materialia* [Article] 62:129-40.

[21]   Bardel D, Perez M, Nelias D, Dancette S, Chaudet P, Massardier V. Cyclic behaviour of a 6061 aluminium alloy: Coupling precipitation and elastoplastic modelling. 2015 *Acta Materialia* [Article] 83:256-68.

[22]   Chen Q, Jeppsson J, Ågren J. Analytical treatment of diffusion during precipitate growth in multicomponent systems. 2008 *Acta Materialia* 56(8):1890-6.

[23]   Gandin CA, Jacot A. Modeling of precipitate-free zone formed upon homogenization in a multi-component alloy. 2007 *Acta Materialia* 55(7):2539-53.

[24]   Rougier L, Jacot A, Gandin CA, Di Napoli P, Thery PY, Ponsen D, et al. Numerical simulation of precipitation in multicomponent Ni-base alloys. 2013 *Acta Materialia* [Article] 61(17):6396-405.

[25]   Du Q, Li Y. An extension of the Kampmann–Wagner numerical model towards as-cast grain size prediction of multicomponent aluminum alloys. 2014 *Acta Materialia* 71(0):380-9.

[26]   Maxwell I, Hellawell A. A simple model for grain refinement during solidification. 1975 *Acta Metall Mater* 23(2):229-37.

[27]   Zhang H, Wang Y, Shang SL, Ravi C, Wolverton C, Chen LQ, et al. Solvus boundaries of (meta)stable phases in the Al–Mg–Si system: First-principles phonon calculations and thermodynamic modeling. 2010 *Calphad* 34(1):20-5.

[28]   Povoden-Karadeniz E, Lang P, Warczok P, Falahati A, Jun W, Kozeschnik E. CALPHAD modeling of metastable phases in the Al–Mg–Si system. 2013 *Calphad* 43(0):94-104.

[29]   Kozeschnik E, Holzer I, Sonderegger B. On the Potential for Improving Equilibrium Thermodynamic Databases with Kinetic Simulations. 2007 *J Phase Equilib Diffus* 28(1):64-71.

[30]   Du Q, Holmedal B, Friis J, Marioara C. Precipitation of Non-spherical Particles in Aluminum Alloys Part II: Numerical Simulation and Experimental Characterization During Aging Treatment of an Al-Mg-Si Alloy. 2015 *Metall and Mat Trans A*:1-11.

[31]   Holmedal B, Osmundsen E, Du Q. Precipitation of Non-Spherical Particles in Aluminum Alloys Part I: Generalization of the Kampmann–Wagner Numerical Model. 2015 *Metall and Mat Trans A*:1-8.

[32]   Myhr O, Grong Ø, Schäfer C. An Extended Age-Hardening Model for Al-Mg-Si Alloys Incorporating the Room-Temperature Storage and Cold Deformation Process Stages. 2015 *Metall and Mat Trans A* 46(12):6018-39.

[33]   Feufel H, Gödecke T, Lukas HL, Sommer F. Investigation of the Al□Mg□Si system by experiments and thermodynamic calculations. 1997 *J Alloy Compd* 247(1–2):31-42.

[34]   Tang Y, Du Y, Zhang L, Yuan X, Kaptay G. Thermodynamic description of the Al–Mg–Si system using a new formulation for the temperature dependence of the excess Gibbs energy. 2012 *Thermochimica Acta* 527:131-42.

[35]   J.P. H. Motreal: Ecole Polytechnique; 2006.

[36]   Bahrami A, Miroux A, Sietsma J. An Age-Hardening Model for Al-Mg-Si Alloys Considering Needle-Shaped Precipitates. 2012 *Metallurgical and Materials Transactions a-Physical Metallurgy and Materials Science* 43A(11):4445-53.

[37]   Myhr OR, Grong O, Pedersen KO. A Combined Precipitation, Yield Strength, and Work Hardening Model for Al-Mg-Si Alloys. 2010 *Metallurgical and Materials Transactions a-Physical Metallurgy and Materials Science* [Article] 41A(9):2276-89.

[38]   Du Y, Chang YA, Huang BY, Gong WP, Jin ZP, Xu HH, et al. Diffusion coefficients of some solutes in fcc and liquid Al: critical evaluation and correlation. 2003 *Materials Science and Engineering a-Structural Materials Properties Microstructure and Processing* [Article] 363(1-2):140-51.